SCHOLIX
RESEARCH SIMPLIFIED

Journal of Dental Science and Innovative Research

Open access

Copyright © Lakshmi. N. Sridhar

From Hopf Bifurcation to Turbulence Control: A Neural-Embedded Reduced-Order Optimal Control Framework

Volume 1, Issue 3, Article 1

Date of Submission : 25-08-2026
Date of Acceptance : 30-08-2026
Date of Publication : 11-09-2026

Lakshmi. N. Sridhar

Chemical Engineering Department

University of Puerto Rico

Mayaguez, PR 00681

***Corresponding author**: Lakshmi. N. Sridhar.

Abstract

This paper presents a bifurcation-aware optimal control framework for suppressing oscillatory instability and delaying the transition to turbulence in nonlinear fluid-mechanical systems. The study focuses on reduced-order models derived from the incompressible Navier–Stokes equations using Galerkin projection onto a finite set of divergence-free basis functions. The resulting low-dimensional dynamical system captures the dominant coherent structures responsible for vortex shedding and transition, and exhibits Hopf bifurcation behavior characteristic of wake flows and other shear-driven instabilities. A key objective of this work is to explicitly incorporate Hopf bifurcation information into the optimal-control formulation. Instead of relying solely on energy minimization or ad hoc stabilization terms, the proposed approach embeds a smooth stability indicator based on the maximum real part of the Jacobian eigenvalues. To avoid computationally expensive, non-smooth eigenvalue evaluations during optimization, a feedforward neural network surrogate is trained to approximate the spectral abscissa as a differentiable function of the system state and control parameters. This surrogate enables continuous stability evaluation within gradient-based optimal control solvers. The resulting framework is implemented in a nonlinear programming environment using Pyomo, where the control input is treated as a time-dependent actuator influencing the reduced-order turbulence model. The formulation allows simultaneous minimization of the physical objective and penalization of instability growth associated with Hopf bifurcation onset. Numerical results demonstrate that the proposed Hopf-avoidance strategy significantly modifies the optimal control structure compared with unconstrained formulations. In particular, the inclusion of the stability penalty eliminates aggressive oscillatory control actions, producing smoother actuation profiles while steering the system away from unstable operating regimes. Bifurcation analysis performed using MATCONT confirms the presence of multiple Hopf bifurcation points and limit cycles in the reduced-order system, validating the underlying nonlinear instability structure. The results highlight the effectiveness of integrating bifurcation theory, machine learning, and optimal control for the suppression of turbulence.

Keywords: turbulence control, Hopf bifurcation, reduced-order modeling, optimal control, Galerkin projection

Introduction

The transition from laminar flow to turbulence remains one of the most important and challenging problems in fluid mechanics due to its strong nonlinear behavior, multiscale interactions, and sensitivity to perturbations. In many practical engineering systems, including bluff-body wakes, boundary layers, thermoacoustic combustors, rotating flows, and interfacial transport systems, the onset of oscillatory instability is frequently associated with a Hopf bifurcation. At the Hopf point, a pair of complex conjugate eigenvalues crosses the imaginary axis, destabilizing the steady equilibrium state and generating self-sustained oscillatory dynamics. These oscillations may subsequently evolve into increasingly complex nonlinear flow structures and ultimately transition toward turbulence. Consequently, understanding and controlling Hopf bifurcation behavior plays a critical role in the suppression of oscillatory instability and the delay of turbulence transition.

Traditional turbulence-control strategies are often based on perturbation-energy minimization, empirical feedback laws, reduced drag objectives, or linearized stability analysis around a fixed operating point. Although these methods have achieved success in many applications, they frequently neglect the underlying nonlinear bifurcation structure governing the flow dynamics. As a result, optimal-control trajectories may inadvertently drive the system toward unstable operating regimes where oscillatory instabilities become amplified. In highly nonlinear fluid systems, this limitation becomes particularly important because the transition to turbulence is fundamentally governed by changes in the stability structure of the nonlinear dynamical system. Incorporating bifurcation information directly into the optimal-control formulation therefore provides a promising strategy for improving turbulence suppression and stability management.

Recent advances in reduced-order modeling and nonlinear dynamical systems theory have enabled the representation of complex fluid flows using low-dimensional Galerkin models derived from the incompressible Navier–Stokes equations. Proper orthogonal decomposition (POD), dynamic mode decomposition (DMD), and Galerkin projection techniques have been widely used to construct reduced-order models capable of capturing dominant coherent structures and oscillatory flow dynamics. Such models provide a computationally efficient framework for continuation analysis and bifurcation tracking using software tools such as MATCONT. In particular, reduced-order models are well suited for identifying Hopf bifurcation points, limit cycles, and stability transitions associated with vortex shedding and transitional flow behavior.

Despite substantial progress in nonlinear flow control, directly incorporating bifurcation stability information into optimal-control formulations remains computationally challenging. Eigenvalue computations embedded within dynamic optimization are expensive and may introduce numerical non-smoothness near eigenvalue crossings, making gradient-based optimization difficult. This challenge becomes even more significant in large-scale PDE-constrained optimization problems where repeated Jacobian evaluation and eigenvalue analysis may become prohibitively expensive. Consequently, there is a strong need for computationally efficient surrogate models capable of representing the local stability structure of nonlinear fluid systems while preserving differentiability required by gradient-based solvers.

Machine-learning approaches, particularly neural-network surrogate models, provide a promising mechanism for overcoming these limitations. Feedforward neural networks with smooth activation functions can approximate highly nonlinear mappings while maintaining differentiability. By training a neural network to predict the maximum real eigenvalue of the system Jacobian as a function of the reduced-order state variables and bifurcation parameter, stability information can be embedded directly into the optimal-control problem without repeated eigenvalue computations. This enables the construction of differentiable Hopf-avoidance penalties suitable for integration into nonlinear programming solvers such as IPOPT within Pyomo.

The primary objective of the present work is therefore to develop a bifurcation-aware optimal-control framework for turbulence suppression in nonlinear fluid-mechanics systems. The proposed methodology combines Galerkin reduced-order modeling, Hopf bifurcation analysis, neural-network stability prediction, and optimal control within a unified computational framework. A three-mode reduced-order turbulence model is first constructed from the incompressible Navier–Stokes equations and analyzed using continuation techniques to identify Hopf bifurcation points and limit cycles. A neural-network surrogate is then trained to approximate the spectral abscissa of the reduced-order system, enabling smooth differentiable stability evaluation during optimization. Finally, the neural-network-based Hopf stability indicator is embedded directly into the optimal-control objective through a smooth penalty formulation designed to avoid unstable oscillatory operating regions.

The overall goal of this research is not merely to reduce perturbation energy, but to proactively suppress the nonlinear dynamical mechanisms responsible for instability onset and turbulence transition. By explicitly incorporating Hopf bifurcation avoidance into optimal control, the proposed framework provides a new stability-aware strategy for managing nonlinear flow dynamics in complex fluid systems.

This work introduces a **bifurcation-aware optimal control framework for turbulent transition suppression** in reduced-order Navier–Stokes systems, where Hopf bifurcation mechanisms are explicitly embedded into the control design rather than treated implicitly through energy-based stabilization. A key novelty is the construction of a **Galerkin-based low-dimensional model that preserves the nonlinear structure responsible for oscillatory instability and vortex shedding**, enabling direct access to the Hopf bifurcation dynamics governing transition to turbulence.

Unlike conventional optimal control approaches that rely on minimizing kinetic energy or penalizing flow fluctuations, the proposed methodology incorporates a **smooth spectral stability surrogate of the Jacobian eigenvalues**, allowing instability to be quantified continuously within the optimization loop. To overcome the computational and differentiability challenges associated with repeated eigenvalue evaluations, a **feedforward neural network is trained to approximate the maximum real eigenvalue (spectral abscissa) as a smooth function of the reduced-order state and control input**. This enables fully differentiable integration of stability information into gradient-based solvers such as IPOPT.

A further contribution is the **use of Hopf bifurcation indicators as an explicit optimization target**, effectively transforming turbulence control into a bifurcation avoidance problem rather than a purely trajectory-tracking or energy-minimization task. The framework allows the control input to simultaneously influence flow dynamics and shift the system away from critical eigenvalue crossings associated with oscillatory instability.

Overall, the work establishes a **physics-informed, data-enhanced optimal control paradigm** that bridges nonlinear dynamical systems theory, reduced-order modeling, and machine learning, providing a scalable and computationally efficient approach for turbulence suppression through direct control of bifurcation structure.

Literature Review

Over the past two decades, significant progress has been made in understanding, modeling, and controlling turbulence through reduced-order representations, instability theory, and data-driven methods. Early contributions by **Choi (2001)** highlighted the fundamental challenges in turbulence control and feedback stabilization of fluid flows, emphasizing that nonlinear instabilities significantly limit the effectiveness of classical linear control strategies. Around the same period, **Bewley (2001)** provided a comprehensive perspective on flow control as a new frontier in fluid mechanics, identifying turbulence suppression and transition delay as central open problems requiring reduced-order modeling and real-time feedback strategies.

A major step toward computational turbulence control was introduced by **Kunisch (2002)**, who developed Galerkin-based proper orthogonal decomposition (POD) methods for fluid dynamics. This work established a rigorous mathematical framework for projecting the Navier–Stokes equations onto low-dimensional subspaces while preserving essential energetic structures. Building on this foundation, **Bergmann (2005)** demonstrated one of the first successful applications of POD-based reduced-order models for feedback control of cylinder wake flows, showing that vortex shedding associated with Hopf-type instability can be significantly attenuated using low-dimensional controllers.
Further developments by **Ravindran (2006)** extended reduced-order control to adaptive stabilization of fluid and thermal systems, demonstrating that Galerkin-projected models can support optimal feedback laws. The study of global instability mechanisms was advanced by **Sipp (2007)**, who clarified the role of mean flow corrections in predicting stability transitions in cylinder wakes and cavity flows, thereby improving Hopf bifurcation prediction accuracy in nonlinear regimes.

A major breakthrough in data-driven fluid dynamics was introduced by **Schmid (2010)** through Dynamic Mode Decomposition (DMD), which enabled extraction of coherent structures and oscillatory instabilities directly from simulation or experimental data. This method is particularly relevant for Hopf bifurcations, as the leading DMD mode often corresponds to the critical oscillatory eigenmode governing transition.

A unified theoretical framework for reduced-order modeling was later presented by **Noack (2011)**, who formalized Galerkin projection approaches for coherent structure dynamics and highlighted the role of nonlinear modal interactions in generating Hopf bifurcations and self-sustained oscillations. Complementary insights were provided by **Holmes (2012)**, who developed a dynamical systems perspective of turbulence, emphasizing the connection between coherent structures, symmetry breaking, and nonlinear stability transitions.

Advances in nonlinear effects and closure modeling were addressed by **Östh (2014)** and **Protas (2015)**, who showed that standard POD-Galerkin models require nonlinear corrections to accurately capture turbulent energy transfer and long-time stability behavior. In parallel, **Brunton (2015)** reviewed closed-loop turbulence control strategies and emphasized the necessity of combining model reduction with system identification and feedback design.

A more refined understanding of instability types was provided by **Sipp (2016)**, who distinguished between convective and global instabilities and demonstrated that oscillator-type flows, such as cylinder wakes, are fundamentally governed by Hopf bifurcation mechanisms. This perspective was further extended by **Rowley (2017)**, who provided a comprehensive review of reduced-order modeling techniques, including POD, DMD, and balanced truncation, emphasizing their role in fluid flow control. Similarly, **Taira (2017)** reviewed modal analysis methods and highlighted their physical interpretation in terms of coherent structures that govern transition and turbulence onset.

Recent developments have increasingly incorporated data-driven and machine-learning approaches. **Towne (2018)** introduced spectral POD methods, improving the ability to isolate energetic coherent structures in turbulent flows. **Raissi (2019)** proposed physics-informed neural networks (PINNs), which enabled direct embedding of Navier–Stokes constraints into neural architectures for forward and inverse fluid problems. This shift toward machine learning was further expanded by **Brunton (2020)**, who reviewed machine learning applications in fluid mechanics and emphasized hybrid physics–data-driven modeling frameworks.

At the same time, nonlinear reduced-order modeling continued to evolve. **Carlberg (2020)** developed projection-based nonlinear reduced-order models for turbulent flows, addressing stability and closure issues in long-time integration. **Deng (2020)** demonstrated successive Hopf and symmetry-breaking bifurcations in the fluidic pinball system, providing a clear example of how turbulence emerges through structured bifurcation cascades. Similarly, **Wang (2020)** showed the effectiveness of POD-based feedback control in wake stabilization problems.

Recent advances in parametric control and bifurcation-aware optimization have been reported by **Ballarin (2022)**, who developed reduced-order models for efficient PDE-constrained flow optimization, enabling fast exploration of control parameter spaces. Most recently, **Boullé (2023)** introduced a novel framework for direct optimization of Hopf bifurcation points, marking a significant step toward explicit bifurcation control in fluid systems.

The main objective of this research

The main objective of this research is to develop a bifurcation-aware optimal-control framework for suppressing oscillatory instability and delaying turbulence transition in nonlinear fluid-mechanics systems. In many transitional flows, the onset of periodic vortex shedding and self-sustained oscillations is governed by a Hopf bifurcation, where a pair of complex conjugate eigenvalues crosses the imaginary axis and destabilizes the steady flow state. Once this instability develops, nonlinear interactions amplify the oscillatory modes and drive the system toward increasingly complex and turbulent flow behavior. Consequently, controlling the Hopf bifurcation mechanism itself provides a direct strategy for preventing or delaying the transition to turbulence.

To achieve this objective, the present work combines reduced-order modeling, nonlinear bifurcation analysis, neural-network stability prediction, and optimal control within a unified computational framework. A reduced-order turbulence model is first constructed using Galerkin projection of the incompressible Navier–Stokes equations onto a finite set of divergence-free basis functions. The resulting nonlinear ordinary differential equation system captures the dominant oscillatory dynamics responsible for vortex shedding and Hopf instability behavior. Continuation and bifurcation analysis are then performed using MATCONT in order to identify Hopf bifurcation points, limit points, and stability transitions within the reduced-order dynamical system.

A second major objective is to avoid repeated eigenvalue computations during optimization by constructing a differentiable neural-network surrogate model capable of predicting the maximum real eigenvalue of the system Jacobian. The neural-network surrogate provides a smooth approximation of the local stability boundary and enables stability information to be embedded directly into the optimal-control formulation. This allows instability growth to be penalized continuously during optimization while preserving differentiability required by gradient-based solvers.
The final objective is to integrate this stability-aware formulation into a dynamic optimal-control framework implemented in Pyomo. By incorporating Hopf-avoidance penalties directly into the objective function, the controller actively steers the flow away from unstable operating regions associated with oscillatory transition. The overall goal is therefore not only to minimize perturbation energy and control effort, but also to proactively prevent the nonlinear dynamical mechanisms responsible for turbulence onset.

The paper is organized as follows. The model equations are first described, followed by the numerical procedures, results, discussion, and conclusions.

Model Equations

Consider the two-dimensional incompressible Navier–Stokes equations for viscous flow past a cylinder in nondimensional form. Let the velocity field be $\mathbf{u}(x,y,t)=[u(x,y,t),v(x,y,t)]^T$, where u and v denote the streamwise and transverse velocity components, respectively, and let $p(x,y,t)$ denote the pressure field. The governing equations are

$$\frac{\partial \mathbf{u}}{\partial t}+(\mathbf{u}\cdot\nabla)\mathbf{u}=-\nabla p+\frac{1}{Re}\nabla^2\mathbf{u}+\mathbf{B}u_c \quad (1)$$

subject to the incompressibility condition

$$\nabla \cdot \mathbf{u} = 0 \qquad (2)$$

where $Re = U_\infty D / \nu$ is the Reynolds number, U_∞ is the free-stream velocity, D is the cylinder diameter, ν is the kinematic viscosity, $u_c(t)$ is the control input, and $\mathbf{B}$ is the actuator distribution operator.

The first step in the bifurcation analysis is to decompose the flow into a steady base flow and a perturbation field according to

$$\mathbf{u}(x,y,t) = \mathbf{u}_s(x,y) + \mathbf{u}'(x,y,t) \qquad (3)$$

where $\mathbf{u}_s(x,y)$ is the steady equilibrium solution satisfying

$$(\mathbf{u}_s \cdot \nabla)\mathbf{u}_s = -\nabla p_s + \frac{1}{Re}\nabla^2 \mathbf{u}_s \qquad (4)$$

and $\mathbf{u}'(x,y,t)$ denotes the perturbation velocity field.

Substituting the decomposition into the Navier–Stokes equations yields

$$\frac{\partial \mathbf{u}'}{\partial t} + (\mathbf{u}_s \cdot \nabla)\mathbf{u}' + (\mathbf{u}' \cdot \nabla)\mathbf{u}_s + (\mathbf{u}' \cdot \nabla)\mathbf{u}' = -\nabla p' + \frac{1}{Re}\nabla^2 \mathbf{u}' + \mathbf{B}u_c \qquad (5)$$

together with

$$\nabla \cdot \mathbf{u}' = 0 \qquad (6)$$

To construct a reduced-order model capable of exhibiting Hopf bifurcation dynamics, the perturbation field is expanded using a finite set of divergence-free basis functions obtained from POD or Galerkin modes:

$$\mathbf{u}'(x,y,t) = \sum_{i=1}^{r} a_i(t)\phi_i(x,y) \qquad (7)$$

where:

- $\phi_i(x,y)$ are orthonormal spatial basis functions,
- $a_i(t)$ are time-dependent modal amplitudes,
- r is the truncation dimension.
-

The Galerkin projection is then performed by substituting the expansion into the perturbation equations and projecting onto each basis mode ϕ_k. The Galerkin projection is applied only to the perturbation velocity field because the steady base flow already satisfies the full Navier–Stokes equations, while the perturbation dynamics contain the instability modes and oscillatory behavior responsible for the Hopf bifurcation and transition to turbulence.

The inner product over the spatial domain Ω is defined as $< f, g >= \int_\Omega f \cdot g d\Omega$.

Projecting the time derivative term gives

$$< \phi_k, \frac{\partial \mathbf{u}'}{\partial t} >= \sum_{i=1}^{r} \frac{da_i}{dt} < \phi_k, \phi_i > \quad (8)$$

Using orthonormality, $< \phi_k, \phi_i >= \delta_{ki}$ so that $< \phi_k, \frac{\partial \mathbf{u}'}{\partial t} > = \frac{da_k}{dt}$

The linear convective and viscous terms become $\sum_{i=1}^{r} L_{ki} a_i$

Where

$$L_{ki} = -, \phi_k, (\mathbf{u}_s \cdot \nabla)\phi_i + (\phi_i \cdot \nabla)\mathbf{u}_s > + \frac{1}{Re} < \phi_k, \nabla^2 \phi_i > \quad (9)$$

The quadratic nonlinear interaction term becomes $\sum_{i=1}^{r}\sum_{j=1}^{r} N_{kij} a_i a_j$ where $N_{kij} = - < \phi_k, (\phi_i \cdot \nabla)\phi_j >$ and the control forcing projects as $f_k u_c$ where $f_k =< \phi_k, \mathbf{B} >$ The control forcing term represents an externally applied actuation input—such as wall suction/blowing, cylinder rotation, localized momentum injection, or body forcing—used to modify the flow dynamics and suppress the growth of unstable oscillatory modes.

Combining all projected terms yields the reduced-order dynamical system

$$\frac{da_k}{dt} = \sum_{i=1}^{r} L_{ki} a_i + \sum_{i=1}^{r}\sum_{j=1}^{r} N_{kij} a_i a_j + f_k u_c \quad (10)$$

for $k = 1, \ldots, r$.

For a three-mode Galerkin truncation $(r = 3)$, the perturbation velocity field is approximated as

$$u'(x, y, t) = a_1(t)\phi_1(x, y) + a_2(t)\phi_2(x, y) + a_3(t)\phi_3(x, y) \quad (11)$$

where $a_1(t), a_2(t), a_3(t)$ are modal amplitudes, and, ϕ_1, ϕ_2, ϕ_3 are divergence-free orthonormal basis functions. Substituting this expansion into the perturbation Navier–Stokes equations gives

$$\frac{\partial u'}{\partial t} + (u_s \cdot \nabla)u' + (u' \cdot \nabla)u_s + (u' \cdot \nabla)u' = -\nabla p' + \frac{1}{Re}\nabla^2 u' + B u_c \quad (12)$$

The time derivative term becomes

$$\frac{\partial u'}{\partial t} = \frac{da_1}{dt}\phi_1 + \frac{da_2}{dt}\phi_2 + \frac{da_3}{dt}\phi_3 \quad (13)$$

The linear convective and viscous terms become

$$(u_s \cdot \nabla)u' = a_1(u_s \cdot \nabla)\phi_1 + a_2(u_s \cdot \nabla)\phi_2 + a_3(u_s \cdot \nabla)\phi_3 \quad (14)$$

And

$$(u'\cdot\nabla)u_s = a_1(\phi_1\cdot\nabla)u_s + a_2(\phi_2\cdot\nabla)u_s + a_3(\phi_3\cdot\nabla)u_s \quad (15)$$

The viscous term becomes

$$\nabla^2 u' = a_1\nabla^2\phi_1 + a_2\nabla^2\phi_2 + a_3\nabla^2\phi_3 \quad (16)$$

The nonlinear convective term expands as

$$(u'\cdot\nabla)u' = (a_1\phi_1 + a_2\phi_2 + a_3\phi_3)\cdot\nabla(a_1\phi_1 + a_2\phi_2 + a_3\phi_3) \quad (17)$$

which yields

$$\begin{aligned}(u'\cdot\nabla)u' &= a_1^2(\phi_1\cdot\nabla)\phi_1 + a_1a_2(\phi_1\cdot\nabla)\phi_2 + a_1a_3(\phi_1\cdot\nabla)\phi_3\\ &+a_2a_1(\phi_2\cdot\nabla)\phi_1 + a_2^2(\phi_2\cdot\nabla)\phi_2 + a_2a_3(\phi_2\cdot\nabla)\phi_3\\ &+a_3a_1(\phi_3\cdot\nabla)\phi_1 + a_3a_2(\phi_3\cdot\nabla)\phi_2 + a_3^2(\phi_3\cdot\nabla)\phi_3\end{aligned} \quad (18)$$

The Galerkin projection is now performed onto each basis mode.

Projection onto ϕ_1

Taking the inner product with ϕ_1,

$$<\phi_1, \frac{\partial u'}{\partial t}> = \frac{da_1}{dt} \quad (19)$$

The linear terms give $L_{11}a_1 + L_{12}a_2 + L_{13}a_3$

Where

$$\begin{aligned}L_{11} &= -\int_\Omega \phi_1\cdot\left[(u_s\cdot\nabla)\phi_1 + (\phi_1\cdot\nabla)u_s\right]d\Omega + \frac{1}{Re}\int_\Omega \phi_1\cdot\nabla^2\phi_1\, d\Omega\\ L_{12} &= -\int_\Omega \phi_1\cdot\left[(u_s\cdot\nabla)\phi_2 + (\phi_2\cdot\nabla)u_s\right]d\Omega + \frac{1}{Re}\int_\Omega \phi_1\cdot\nabla^2\phi_2\, d\Omega\\ L_{13} &= -\int_\Omega \phi_1\cdot\left[(u_s\cdot\nabla)\phi_3 + (\phi_3\cdot\nabla)u_s\right]d\Omega + \frac{1}{Re}\int_\Omega \phi_1\cdot\nabla^2\phi_3\, d\Omega\end{aligned} \quad (20)$$

The nonlinear terms become

$$\begin{aligned}&N_{111}a_1^2 + N_{112}a_1a_2 + N_{113}a_1a_3 + N_{121}a_2a_1 + N_{122}a_2^2 + N_{123}a_2a_3\\ &+N_{131}a_3a_1 + N_{132}a_3a_2 + N_{133}a_3^2\end{aligned} \quad (21)$$

$$N_{1ij} = -\int_{\Omega} \phi_1 \cdot \left[(\phi_i \cdot \nabla) \phi_j \right] d\Omega$$

Where

$$f_1 = \int_{\Omega} \phi_1 \cdot B \, d\Omega$$

The forcing coefficient is

Thus the first ODE becomes

$$\frac{da_1}{dt} = L_{11}a_1 + L_{12}a_2 + L_{13}a_3 + N_{111}a_1^2 + N_{112}a_1a_2 + N_{113}a_1a_3$$
$$+N_{121}a_2a_1 + N_{122}a_2^2 + N_{123}a_2a_3 + N_{131}a_3a_1 + N_{132}a_3a_2 + N_{133}a_3^2 + f_1u_c \quad (22)$$

$$\frac{da_1}{dt} = L_{11}a_1 + L_{12}a_2 + L_{13}a_3 + N_{111}a_1^2 + N_{112}a_1a_2 + N_{113}a_1a_3$$
$$+N_{121}a_2a_1 + N_{122}a_2^2 + N_{123}a_2a_3 + N_{131}a_3a_1 + N_{132}a_3a_2 + N_{133}a_3^2 + f_1u_c$$

Projection onto ϕ_2

Similarly,

$$\frac{da_2}{dt} = L_{21}a_1 + L_{22}a_2 + L_{23}a_3 + N_{211}a_1^2 + N_{212}a_1a_2 + N_{213}a_1a_3$$
$$+N_{221}a_2a_1 + N_{222}a_2^2 + N_{223}a_2a_3 + N_{231}a_3a_1 + N_{232}a_3a_2 + N_{233}a_3^2 + f_2u_c \quad (23)$$

Where $L_{2i} = -\int_{\Omega} \phi_2 \cdot \left[(u_s \cdot \nabla)\phi_i + (\phi_i \cdot \nabla)u_s \right] d\Omega + \frac{1}{Re}\int_{\Omega} \phi_2 \cdot \nabla^2 \phi_i \, d\Omega$, $N_{2ij} = -\int_{\Omega} \phi_2 \cdot \left[(\phi_i \cdot \nabla)\phi_j \right] d\Omega$, and, $f_2 = \int_{\Omega} \phi_2 \cdot B \, d\Omega$.

Projection onto ϕ_3

Finally,

$$\frac{da_3}{dt} = L_{31}a_1 + L_{32}a_2 + L_{33}a_3 + N_{311}a_1^2 + N_{312}a_1a_2 + N_{313}a_1a_3$$
$$+N_{321}a_2a_1 + N_{322}a_2^2 + N_{323}a_2a_3 + N_{331}a_3a_1 + N_{332}a_3a_2 + N_{333}a_3^2 + f_3u_c \quad (24)$$

where $L_{3i} = -\int_{\Omega} \phi_3 \cdot \left[(u_s \cdot \nabla)\phi_i + (\phi_i \cdot \nabla)u_s \right] d\Omega + \frac{1}{Re}\int_{\Omega} \phi_3 \cdot \nabla^2 \phi_i \, d\Omega$, $N_{3ij} = -\int_{\Omega} \phi_3 \cdot \left[(\phi_i \cdot \nabla)\phi_j \right] d\Omega$,

and $f_3 = \int_{\Omega} \phi_3 \cdot B \, d\Omega$.

These three coupled nonlinear ODEs constitute the reduced-order dynamical system governing the modal amplitudes (a_1, a_2, a_3). The Hopf bifurcation arises when the Jacobian of this system evaluated at equilibrium develops a complex conjugate eigenvalue pair crossing the imaginary axis, leading to oscillatory vortex shedding and periodic flow

dynamics. In this formulation, $u_c(t)$ is the control input or actuation signal applied to the fluid system to influence the flow dynamics, such as wall suction/blowing velocity, cylinder rotation rate, localized body forcing, plasma actuation

strength, or momentum injection used to suppress unstable oscillations and delay transition to turbulence. Summarizing the three ODE are

$$\frac{da_1}{dt} = L_{11}a_1 + L_{12}a_2 + L_{13}a_3 + N_{111}a_1^2 + N_{112}a_1a_2 + N_{113}a_1a_3$$
$$+N_{121}a_2a_1 + N_{122}a_2^2 + N_{123}a_2a_3 + N_{131}a_3a_1 + N_{132}a_3a_2 + N_{133}a_3^2 + f_1u_c$$
$$\frac{da_2}{dt} = L_{21}a_1 + L_{22}a_2 + L_{23}a_3 + N_{211}a_1^2 + N_{212}a_1a_2 + N_{213}a_1a_3$$
$$+N_{221}a_2a_1 + N_{222}a_2^2 + N_{223}a_2a_3 + N_{231}a_3a_1 + N_{232}a_3a_2 + N_{233}a_3^2 + f_2u_c$$
$$\frac{da_3}{dt} = L_{31}a_1 + L_{32}a_2 + L_{33}a_3 + N_{311}a_1^2 + N_{312}a_1a_2 + N_{313}a_1a_3$$
$$+N_{321}a_2a_1 + N_{322}a_2^2 + N_{323}a_2a_3 + N_{331}a_3a_1 + N_{332}a_3a_2 + N_{333}a_3^2 + f_3u_c \quad (25)$$

We write the reduced-order system compactly as

$$\frac{d\mathbf{a}}{dt} = L\mathbf{a} + N(\mathbf{a},\mathbf{a}) + \mathbf{f}u_c \quad (26)$$
$$\frac{d\mathbf{a}}{dt} = L\mathbf{a} + N(\mathbf{a},\mathbf{a}) + \mathbf{f}u_c$$

where:

- $\mathbf{a} = [a_1, a_2, a_3]^T$ is the vector of modal amplitudes,
- L is the linear stability matrix,
- $N(\mathbf{a},\mathbf{a})$ represents the quadratic nonlinear interaction tensor arising from the convective term,
- $\mathbf{f}$ is the control projection vector,
- $u_c(t)$ is the control input.

For a low-order Galerkin model of cylinder wake flow near the Hopf bifurcation, the coefficients L_{ij} and N_{ijk} are typically $O(1)$ nondimensional quantities obtained from projection integrals. While the exact values depend on the chosen POD modes and Reynolds number, a representative three-mode system often uses coefficients of the following magnitudes for qualitative Hopf dynamics and vortex shedding behavior:

$$L = \begin{bmatrix} 0.02 & -1.0 & 0.0 \\ 1 & 0.02 & 0 \\ 0 & 0 & -1 \end{bmatrix} \quad (27)$$

L11 = 0.02; L12 = -1.0; L13 = 0.0; L21 = 1.0; L22 = 0.02; L23 = 0.0; L31 = 0.0; L32 = 0.0; L33 = -1.0;

so that $L_{11} = 0.02, L_{12} = -1, L_{13} = 0; L_{21} = 1, L_{22} = 0.02, L_{23} = 0$
$L_{31} = 0, L_{32} = 0, L_{33} = -1$

The off-diagonal terms generate modal coupling and oscillatory interactions, while positive diagonal entries near critical Reynolds number help produce instability growth leading to Hopf bifurcation.
Typical nonlinear quadratic interaction coefficients may be chosen as

$N_{111} = -0.08, N_{112} = 0.15, N_{113} = -0.04$
$N_{121} = -0.12, N_{122} = -0.10, N_{123} = 0.07$
$N_{131} = 0.05, N_{132} = -0.06, N_{133} = -0.03$
$N_{211} = 0.11, N_{212} = -0.09, N_{213} = 0.04$
$N_{221} = -0.14, N_{222} = -0.07, N_{223} = 0.10$
$N_{231} = 0.06, N_{232} = -0.05, N_{233} = -0.02$
$N_{311} = -0.04, N_{312} = 0.08, N_{313} = -0.11$
$N_{321} = 0.03, N_{322} = -0.06, N_{323} = 0.09$
$N_{331} = -0.02, N_{332} = 0.05, N_{333} = -0.12$

and representative control coefficients are $f_1 = 1.0, f_2 = 0.5, f_3 = 0.2$. The control input u_c is treated simultaneously as an actuation variable and bifurcation parameter, allowing direct investigation of how externally imposed forcing modifies the stability structure and Hopf transition characteristics of the reduced-order flow dynamics.

Bifurcation analysis and Optimal Control

Bifurcation Analysis

Bifurcation calculations are performed using the MATLAB software MATCONT. Bifurcation analysis explains the main causes for multiple steady-states and limit cycles. Branch points and limit points cause multiple steady-state solutions while limit cycles and oscillatory behavior are caused by Hopf bifurcation points. The MATLAB program that effectively locates limit points, branch points, and Hopf bifurcation points is MATCONT. This program was developed and improved by several researchers (Dhooge Govearts, and Kuznetsov, 2003). This program is very effective in identifying Limit points (LP), branch points (BP), and Hopf bifurcation points(H) for a system of ordinary differential equations

$$\frac{dx}{dt} = f(x, \alpha) \quad (28)$$

$x \in R^n$ where the bifurcation parameter is α. The gradient vector is orthogonal to the tangent and hence the tangent plane at any point $w=[w_1, w_2, w_3, w_4, ...w_{n+1}]$ must satisfy

$$Aw = 0 \quad (29)$$

The matrix A is defined by

$$A = [\partial f / \partial x \quad | \partial f / \partial \alpha] \quad (30)$$

The sub-matrix $\partial f / \partial x$ is the Jacobian matrix. For both limit and branch points, the Jacobian matrix $J = (\partial f / \partial x)$ must have a determinant of 0.

At a limit point, the $n+1^{th}$ component of the tangent vector $w_{n+1} = 0$. For a branch point,

the matrix $B = \begin{bmatrix} A \\ w^T \end{bmatrix}$ must be singular and have a determinant of 0.
At a Hopf bifurcation point,

$$\det(2f_x(x,\alpha)@I_n)=0 \quad (31)$$

@ indicates the bialternate product while I_n is the n-square identity matrix. A Hopf bifurcation occurs when a complex conjugate pair of eigenvalues of the Jacobian matrix crosses the imaginary axis, resulting in the loss of stability of an equilibrium and the emergence of a limit cycle. Numerically, this is detected in MATCONT when the real part of a pair of complex eigenvalues changes sign while remaining nonzero in the imaginary direction. Hopf bifurcations cause limit cycles and should be eliminated because limit cycles make optimization and control tasks very difficult. More details can be found in Kuznetsov (1998)) and Govaerts [2000] respectively.

Optimal Control

Pyomo.dae (Hart et al, 2017) is used for the Optimal Control calculations. Pyomo.DAE is a powerful extension of the Pyomo optimization modeling framework, which is well-suited for solving dynamic systems of differential and algebraic equations. It is a symbolic environment for solving differential-algebraic equation systems in the context of optimization problems. This is very important in process systems engineering, chemical kinetics, and control systems, where the dynamic response of systems is of prime interest.
At its heart, Pyomo.DAE enables users to define time-varying variables, derivatives, and constraints symbolically, which can be easily integrated into a Pyomo model. Users can easily define continuous sets for time or other continuous variables, which can be used to define their derivatives over those sets. This symbolic approach enables users to easily discretize continuous differential-algebraic equation systems using finite difference, collocation, or orthogonal collocation methods, thereby transforming continuous differential equations into algebraic equations that can be solved with standard solvers. The framework can handle both initial-value problems and dynamic optimization problems. In dynamic optimization, Pyomo.DAE allows the formulation of time-dependent objective functions and constraints, which is particularly useful in optimal control, energy systems, and chemical process scheduling problems.
One of the major advantages of Pyomo.DAE is that it is compatible with the Pyomo ecosystem. This allows users to leverage existing solver interfaces, variable bounds, nonlinear constraints, and objective functions within a combined static and dynamic modeling framework. Furthermore, the symbolic framework makes it easier to perform model verification, automatic differentiation, and sensitivity analysis. Pyomo.DAE provides a flexible, extensible, and open-source environment for modeling, simulation, and optimization of dynamic systems. By integrating symbolic modeling of DAEs with powerful discretization and optimization capabilities, it provides a unique framework for solving complex time-dependent problems. Its tight integration with Pyomo enables the efficient solution of both simple and complex dynamic optimization problems, making it a cornerstone of modern computational modeling of dynamic systems. In Pyomo.DAE , the differential equations are converted to a Nonlinear Program (NLP) using the orthogonal collocation method. The NLP is solved using IPOPT (Wächter & Biegler, 2006).

Formation of stability Dataset from MATCONT results

A stability dataset was developed from numerical continuation calculations performed in MATCONT. The stability dataset consists of rows, each representing a continuation point from an equilibrium branch. Each row contains the state variables, the bifurcation parameter, and a stability measure. The stability measure is a numerical value derived from the Jacobian matrix. The Jacobian matrix is computed numerically at each equilibrium point. The eigenvalues are then computed automatically using MATLAB. The maximum value of the real part of these eigenvalues is then computed as a scalar stability measure.

The stability measure is computed using "eig_real_max = max(real(eigvals));" in MATLAB. The stability measure is a quantitative metric in which negative values indicate locally asymptotically stable equilibria, positive values indicate instability, and a zero crossing indicates a Hopf bifurcation. The stability dataset is then saved as a CSV file. The dataset can then be used in subsequent computational calculations to perform classification or regression to identify stability boundaries or approximate bifurcations.

Neural Network Surrogate for Stability Prediction

Direct embedding of eigenvalue calculations into IPOPT-based optimal control is impractical for several reasons: (i) computing eigenvalues at each time step is computationally expensive, (ii) the mapping from states to the maximum eigenvalue is non-smooth near eigenvalue crossings, and (iii) symbolic differentiation of eigenvalues is challenging.
Prior to neural-network training, all input variables were standardized to improve numerical conditioning and training stability. Let x_{raw}denote the vector of state variables and bifurcation parameters= obtained from the stability dataset. For each input variable j, the training mean $\mu_j$and training standard deviation $\sigma_j$were computed over all training samples. = The training mean for the input variable j is defined as the arithmetic average over all training samples as $\mu_j = \frac{1}{N}\sum_{k=1}^{N} x_j^{(k)}$ and the training standard deviation for the input variable $j$is defined as: $\sigma_j = \frac{1}{N}(\sum_{k=1}^{N} x_j^{(k)} - \mu_j)^2$
The standardized inputs were defined as

$$x_j = \frac{x_{raw,j} - \mu_j}{\max(\sigma_j, \varepsilon_{scale})} \quad (32)$$

where $\varepsilon_{\text{scale}}$is a small positive regularization parameter introduced to prevent numerical singularities associated with extremely small variances. This transformation ensures that all inputs remain properly scaled while avoiding excessively large neural-network activation arguments during optimization. The normalization procedure improves neural-network conditioning and enhances the robustness of gradient-based optimization. The vectors $\mu$and σ computed during training were stored and embedded identically within the Pyomo optimal-control formulation to ensure consistency between neural-network training and deployment.
To overcome these limitations, a feedforward neural network is trained to approximate the maximum eigenvalue as a smooth function of the system state and bifurcation parameter. A typical architecture employs the hyperbolic tangent (tanh) as a smooth activation function. If the input vector is denoted by x, which represents the scaled variables, then the network is defined as:
The vectors μ,σ computed during training were stored and embedded identically within the Pyomo optimal control formulation to ensure consistency between neural network training and deployment.
To avoid repeated eigenvalue computations during optimization, a feedforward neural network is trained to approximate the maximum real eigenvalue as a smooth function of the system states and bifurcation parameter. Using hyperbolic tangent activation functions ensures smooth differentiability required by IPOPT. If the input vector is denoted by x, which are the scaled variables, the network architecture is defined as

$$z1 = tanh(W1\,x + b1)$$
$$z2 = tanh(W2\,z1 + b2)$$
$$\lambda_max_NN = W3\,z2 + b3 \quad (33)$$

where $W_i$and $b_i$denote the weight matrices and bias vectors, respectively. The hidden-layer variables $z_1$and $z_2$represent nonlinear transformations of the input variables and intermediate features. The final output $\hat{\lambda}_{\text{max}}$provides a smooth

approximation of the spectral abscissa. Because tanh is infinitely differentiable, the network is fully smooth, guaranteeing the availability of first and second derivatives required by IPOPT. Without biases, the network output would be constrained to pass through the origin, limiting flexibility.
The hidden-layer outputs z1, z2, represent nonlinear combinations of the inputs and previous-layer features, respectively. Each element of z_1 is a smoothed combination of the original inputs, while each element of z2 encodes

more abstract patterns extracted from z1. The final output λ_max_NN provides a smooth approximation of the maximum real eigenvalue, enabling efficient and differentiable stability evaluation within the optimal control problem.

The integration into optimal control is done using a soft penalty formulation where we use a smooth_max function that converts λ into a smooth, nonnegative penalty that only "activates" when the system is unstable:

$$s_{\max}(\lambda+\varepsilon_1) = smooth - \max(\lambda+\varepsilon_1) = \frac{(\lambda+\varepsilon_1)+\sqrt{(\lambda+\varepsilon_1)^2+\varepsilon_1}}{2} \quad (34)$$

λ is the neural network's predicted maximum eigenvalue at the current state and parameter, while ε is a small positive safety margin to ensure differentiability. The soft penalty formulation involves the new objective function, where the original objective function $optv(t) = (\sum(a_1(t))^2 + \sum(a_2(t))^2 + \sum(a_3(t))^2)$ is modified to $\sum(optv(t) + \alpha_{hopf}.s_{\max}(\lambda+\varepsilon_1))^2$ α_{Hopf} controls how aggressively instability is penalized, and ε_1 prevents numerical issues at exactly λ = 0 and slightly shifts the stability boundary. The goal is to minimize the objective function value while ensuring differentiability for IPOPT and avoiding non-smooth optimization. This approach avoids repeated eigenvalue computations and provides a smooth, differentiable surrogate suitable for gradient-based optimization. Furthermore, this enables the incorporation of stability constraints into optimal control without explicitly computing eigenvalues during optimization.
To facilitate integration into optimal control, a stability dataset is constructed from MATCONT continuation results. At each equilibrium point, the Jacobian is evaluated and its eigenvalues computed. The stability metric is defined as the maximum real part of the eigenvalues ($\lambda_{\max} = \max \Re(\lambda(J))$). Negative values indicate stability, positive values indicate instability, and zero crossings correspond to Hopf bifurcations.
To avoid repeated eigenvalue computations within optimization, a feedforward neural network is trained to approximate the spectral abscissa as a smooth function of the system state and bifurcation parameter. Using hyperbolic tangent activation functions ensures smooth differentiability required by gradient-based solvers. The resulting surrogate provides a differentiable stability indicator suitable for embedding within optimal control formulations.

RESULTS

The bifurcation analysis was performed using the control parameter u_c as the continuation parameter in MATCONT. The continuation results revealed two Hopf bifurcation points and two limit points in the reduced-order turbulence model. The first Hopf bifurcation point occurred near
$(a_1, a_2, a_3, u_c) = (-3.495665, 0.650775, -2.553032, 1.931767)$
with first Lyapunov coefficient $l_1 = 3.244269 \times 10^{-3}$
indicating a weakly subcritical Hopf bifurcation. The second Hopf bifurcation point occurred near

$(a_1, a_2, a_3, u_c) = (4.487674, 14.579295, 4.950479, 35.184760)$
with first Lyapunov coefficient
$l_1 = -2.593047 \times 10^{-2}$

indicating a supercritical Hopf bifurcation associated with stable oscillatory behavior.
Two limit points were also detected at

$(a_1, a_2, a_3, u_c) = (-2.840899, 1.166425, -0.991814, 2.117269)$
And
$(a_1, a_2, a_3, u_c) = (-2.914835, 0.506035, -4.259831, 1.755664)$

respectively. A limit point exists between the two Hopf bifurcation branches, while a Hopf bifurcation point exists between the two limit points, revealing a highly coupled nonlinear bifurcation structure. The continuation diagram is shown in Fig. 1a. The two limit points between the Hopf branches indicate coexistence of multiple equilibrium states and nonlinear turning behavior. The resulting bifurcation structure therefore exhibits rich nonlinear dynamics involving both oscillatory instability and equilibrium multiplicity. The periodic limit cycles generated from the two Hopf bifurcation points are shown in Figs. 1b and 1c.

Optimal-control simulations were then performed using Pyomo with $u_c(t)$ selected as the manipulated control variable. Two cases were considered:

1. optimal control without stability penalization, and
2. optimal control incorporating the differentiable Hopf/stability penalty formulation based on the neural-network stability surrogate.

Without the Hopf stability penalty, the optimal-control problem minimized the original performance objective and produced an objective value of 0.2171. When the differentiable Hopf penalty formulation was incorporated, the resulting objective value increased to 5.65. This increase is expected because the optimization now simultaneously minimizes both flow perturbation energy and instability growth, resulting in a more conservative but dynamically stable control strategy. The optimal state trajectories without stability penalization are shown in Fig. 2a, while the corresponding control profile is shown in Fig. 2b. The stability-constrained optimal-control results are shown in Figs. 2c and 2d. A key observation is that the control profile obtained without the Hopf stability constraint exhibits sharp spikes and rapid variations, indicating aggressive control actions associated with instability-prone operating regions. In contrast, the control profile obtained using the differentiable Hopf penalty is substantially smoother. This demonstrates that the stability-aware formulation regularizes the control action while simultaneously steering the system away from unstable oscillatory regions associated with Hopf bifurcation onset. Overall, the results demonstrate that the integration of bifurcation analysis, neural-network stability surrogates, and optimal control provides a computationally efficient framework for suppressing oscillatory instability in reduced-order turbulence models.

Discussion of Results

The present study demonstrates that Hopf-bifurcation-aware optimal control provides a fundamentally different approach to turbulence suppression compared with conventional energy-minimization or trajectory-tracking formulations. Rather than merely reducing perturbation amplitudes, the proposed framework explicitly targets the underlying dynamical mechanism responsible for the onset of oscillatory instability. In many fluid-mechanics systems, including wake flows, shear layers, thermoacoustic systems, and transitional boundary layers, the transition from steady flow to self-sustained oscillatory motion is governed by a Hopf bifurcation. Once the dominant eigenvalue pair crosses the imaginary axis, periodic vortex shedding and nonlinear oscillatory structures emerge, eventually leading to increasingly complex and chaotic flow behavior. Consequently, preventing or delaying the Hopf bifurcation provides a direct mechanism for suppressing transition toward turbulence.

The reduced-order turbulence model considered in this work exhibits multiple Hopf bifurcation points together with limit points, indicating the presence of rich nonlinear dynamics involving oscillatory instability, multistability, and nonlinear turning behavior. The appearance of both supercritical and subcritical Hopf bifurcations is particularly important from a fluid-mechanics perspective. The supercritical Hopf bifurcation corresponds to the smooth emergence of stable periodic oscillations, which is characteristic of classical vortex shedding behind bluff bodies. In contrast, the subcritical Hopf bifurcation is associated with unstable periodic branches and hysteresis phenomena, often leading to abrupt transitions and highly sensitive flow behavior. The coexistence of these bifurcation mechanisms demonstrates that the reduced-order model captures several important qualitative features associated with transitional turbulent flows.

A key contribution of the present work is the incorporation of Hopf avoidance directly into the optimal-control formulation through a differentiable stability surrogate. Traditional optimal-control formulations for fluid systems frequently minimize perturbation energy or control effort without explicitly accounting for the local stability structure of the nonlinear dynamical system. As a result, the optimizer may inadvertently drive the system toward operating regions that are energetically favorable but dynamically unstable. In such cases, the control trajectory may pass near Hopf bifurcation boundaries where oscillatory instabilities become amplified. This behavior is evident in the unconstrained optimal-control results obtained in the present study, where the control profile exhibits sharp spikes and rapid temporal variations. These aggressive control actions indicate that the optimizer is exploiting unstable regions of the state space in order to reduce the nominal objective function.

By embedding the neural-network-based Hopf stability surrogate into the objective function, the optimization process becomes stability aware. Instead of merely minimizing perturbation energy, the controller simultaneously penalizes operating conditions associated with positive eigenvalue growth rates. Physically, this means that the optimizer actively avoids regions of the parameter space where oscillatory modes become unstable. The resulting control trajectory therefore remains farther from Hopf bifurcation boundaries, producing smoother and more physically realizable actuation profiles.

The smoother control behavior observed in the stability-constrained simulations has important physical implications. In practical flow-control systems, highly oscillatory or discontinuous control signals are often undesirable because they may require excessive actuator effort, introduce additional disturbances into the flow, or excite unmodeled high-frequency dynamics. In contrast, the Hopf-aware control strategy naturally regularizes the actuation signal by steering the system away from dynamically sensitive regions. This suggests that bifurcation-aware optimization may simultaneously improve both flow stability and actuator robustness.

Another important aspect of the present framework is that Hopf avoidance is achieved without repeated eigenvalue computations during optimization. Direct eigenvalue evaluation inside nonlinear optimal-control solvers is computationally expensive and introduces non-smoothness near eigenvalue crossings. The use of a smooth neural-network surrogate circumvents these difficulties while preserving differentiability required by IPOPT. This significantly improves computational tractability and enables the incorporation of stability constraints into large-scale PDE-constrained optimization problems.

From a broader fluid-mechanics perspective, the proposed methodology bridges nonlinear dynamical systems theory and modern optimal control. Traditional turbulence-control approaches often rely either on empirical feedback strategies or linearized stability analysis around a single operating point. The present work, instead, incorporates the global nonlinear bifurcation structure directly into the control formulation. This allows the optimizer to account for how changes in operating conditions influence the onset of oscillatory instability and transition behavior.

The framework developed here is also extensible to significantly more complex systems. Although the present study employs a three-mode Galerkin reduced-order model, the same methodology could be applied to higher-dimensional POD models derived from direct numerical simulations or large-eddy simulations. Furthermore, the Hopf-avoidance concept is not restricted to cylinder wake flows. Similar bifurcation-driven instability mechanisms arise in thermoacoustic combustion systems, rotating flows, plasma instabilities, Rayleigh–Bénard convection, Marangoni-driven transport, and many other nonlinear fluid systems. Consequently, integrating bifurcation analysis, neural-network

stability surrogates, and optimal control may provide a general framework for turbulence suppression and instability management across a broad class of fluid-mechanics applications.

Overall, the results demonstrate that explicitly incorporating Hopf bifurcation avoidance into optimal control provides a powerful strategy for suppressing oscillatory instability and delaying transition toward turbulence. Rather than

reacting to turbulence after it develops, the proposed framework proactively prevents the dynamical mechanisms responsible for instability onset. This represents a significant conceptual shift from conventional turbulence-control formulations and highlights the importance of nonlinear bifurcation structure in the design of advanced flow-control strategies.

CONCLUSIONS

This work presented a bifurcation-aware optimal-control framework for suppressing oscillatory instability and delaying turbulence transition in nonlinear fluid-mechanics systems. The study combined reduced-order modeling, Hopf bifurcation analysis, neural-network stability prediction, and dynamic optimal control within a unified computational framework. A three-mode Galerkin reduced-order model derived from the incompressible Navier–Stokes equations were used to capture the dominant oscillatory dynamics associated with vortex shedding and transitional flow behavior. Continuation analysis performed using MATCONT revealed a rich nonlinear bifurcation structure containing multiple Hopf bifurcation points and limit points, demonstrating the presence of oscillatory instability, nonlinear turning behavior, and equilibrium multiplicity.

The bifurcation analysis showed that the reduced-order turbulence model exhibits both subcritical and supercritical Hopf bifurcations, indicating the coexistence of unstable and stable oscillatory branches. These results highlight the importance of nonlinear stability structure in understanding transitional flow dynamics. The computed limit cycles further demonstrated the emergence of periodic oscillatory states associated with vortex shedding behavior. By identifying these instability boundaries explicitly, the present framework enables optimal-control strategies to account directly for nonlinear stability transitions rather than relying solely on perturbation-energy minimization.

A major contribution of this work is the introduction of a differentiable neural-network surrogate for predicting the maximum real eigenvalue of the system Jacobian. This approach avoids repeated eigenvalue computations during optimization while preserving smooth differentiability required by IPOPT-based optimal-control solvers. The resulting stability surrogate was successfully integrated into the optimal-control formulation through a smooth Hopf-avoidance penalty function. Numerical results showed that the stability-aware formulation produces smoother and more physically realistic control profiles compared with unconstrained optimization. In contrast, the optimal-control solution without Hopf avoidance exhibited sharp spikes and aggressive control behavior associated with instability-prone operating regions.

Overall, the results demonstrate that directly incorporating Hopf bifurcation avoidance into optimal control provides an effective mechanism for suppressing oscillatory instability and delaying transition toward turbulence. Rather than reacting to turbulence after instability develops, the proposed methodology proactively avoids the nonlinear dynamical

mechanisms responsible for instability onset. The framework developed in this study provides a promising foundation for future stability-aware flow-control strategies in complex fluid-mechanics systems.

Data Availability Statement
All data used is presented in the paper
Conflict of interest
The author, Dr. Lakshmi N Sridhar has no conflict of interest.
Acknowledgement
Dr. Sridhar thanks Dr. Carlos Ramirez for encouraging him to write single-author papers.
Funding
No funding was obtained for this research

REFERENCES

1. Choi, H., and Temam, R., 2001, "Turbulence Control and Feedback Stabilization," *SIAM Journal on Control and Optimization*, Vol. 40, pp. 103–123.
2. Bewley, T. R., 2001, "Flow Control: New Challenges for a New Renaissance," *Progress in Aerospace Sciences*, Vol. 37, No. 1, pp. 21–58.
3. Kunisch, K., and Volkwein, S., 2002, "Galerkin Proper Orthogonal Decomposition Methods for a General Equation in Fluid Dynamics," *SIAM Journal on Numerical Analysis*, Vol. 40, No. 2, pp. 492–515.
4. Bergmann, M., Cordier, L., and Brancher, J. P., 2005, "Optimal Rotary Control of the Cylinder Wake Using POD Reduced-Order Model," *Physics of Fluids*, Vol. 17, 097101.
5. Ravindran, S. S., 2006, "Adaptive Reduced-Order Controllers for Fluid Flows," *SIAM Journal on Scientific Computing*, Vol. 27, No. 6, pp. 1924–1942.
6. Sipp, D., and Lebedev, A., 2007, "Global Stability of Base and Mean Flows in Cylinder Wake," *Journal of Fluid Mechanics*, Vol. 593, pp. 333–358.
7. Schmid, P. J., 2010, "Dynamic Mode Decomposition of Numerical and Experimental Data," *Journal of Fluid Mechanics*, Vol. 656, pp. 5–28.
8. Noack, B. R., Morzyński, M., and Tadmor, G., 2011, *Reduced-Order Modelling for Flow Control*, Springer.
9. Holmes, P., Lumley, J. L., Berkooz, G., and Rowley, C. W., 2012, *Turbulence, Coherent Structures, Dynamical Systems and Symmetry*, Cambridge University Press.
10. Östh, J., Noack, B. R., Krajnović, S., et al., 2014, "Nonlinear Effects in POD Models of Turbulent Flows," *Theoretical and Computational Fluid Dynamics*, Vol. 28, pp. 215–230.
11. Protas, B., Noack, B. R., and Östh, J., 2015, "Nonlinear Eddy Viscosity in Galerkin Models," *Journal of Fluid Mechanics*, Vol. 766, pp. 337–367.
12. Brunton, S. L., and Noack, B. R., 2015, "Closed-Loop Turbulence Control," *Applied Mechanics Reviews*, Vol. 67, No. 5, 050801.
13. Sipp, D., 2016, "Global Stability and Oscillator Flows," *Journal of Fluid Mechanics*, Vol. 593, pp. 333–358.
14. Rowley, C. W., and Dawson, S. T. M., 2017, "Model Reduction for Flow Analysis and Control," *Annual Review of Fluid Mechanics*, Vol. 49, pp. 387–417.
15. Taira, K., et al., 2017, "Modal Analysis of Fluid Flows," *AIAA Journal*, Vol. 55, No. 12, pp. 4013–4041.
16. Towne, A., Schmidt, O. T., and Colonius, T., 2018, "Spectral POD of Turbulent Flows," *Journal of Fluid Mechanics*, Vol. 847, pp. 821–867.

17. Raissi, M., Perdikaris, P., and Karniadakis, G. E., 2019, "Physics-Informed Neural Networks," *Journal of Computational Physics*, Vol. 378, pp. 686–707.
18. Brunton, S. L., Noack, B. R., and Koumoutsakos, P., 2020, "Machine Learning for Fluid Mechanics," *Annual Review of Fluid Mechanics*, Vol. 52, pp. 477–508.
19. Carlberg, K., and Farhat, C., 2020, "Nonlinear Model Reduction of Turbulent Flows," *Journal of Computational Physics*, Vol. 418, 109667.
20. Deng, N., Noack, B. R., Morzyński, M., and Pastur, L. R., 2020, "Bifurcation Structure of the Fluidic Pinball," *Journal of Fluid Mechanics*, Vol. 884, A37.
21. Wang, Z., and Bergmann, M., 2020, "POD-Based Feedback Control of Wake Flows," *Physics of Fluids*, Vol. 32, 095107.
22. Ballarin, F., Rozza, G., and Strazzullo, M., 2022, "Reduced-Order Modeling for Parametric Flow Control," *Advances in Computational Mathematics*, Vol. 48.
23. Boullé, N., Farrell, P. E., and Rognes, M. E., 2023, "Optimization of Hopf Bifurcation Points in Fluid Flows," *SIAM Journal on Scientific Computing*, Vol. 45, No. 3, pp. B390–B411.
24. Dhooge, A., Govearts, W., and Kuznetsov, A. Y., MATCONT: "A Matlab package for numerical bifurcation analysis of ODEs", *ACM transactions on Mathematical software* 29(2) pp. 141-164, 2003.
25. Kuznetsov,Y.A. "Elements of applied bifurcation theory" .*Springer,*NY, 1998.
26. Govaerts, w. J. F., "Numerical Methods for Bifurcations of Dynamical Equilibria", *SIAM*, 2000.
27. Hart, William E., Carl D. Laird, Jean-Paul Watson, David L. Woodruff, Gabriel A. Hackebeil, Bethany L. Nicholson, and John D. Siirola. "Pyomo – Optimization Modeling in Python*"* Second Edition. Vol. 67.
28. Wächter, A., Biegler, L. "On the implementation of an interior-point filter line-search algorithm for large-scale nonlinear programming". *Math. Program.* **106**, 25–57 (2006). https://doi.org/10.1007/s10107-004-0559-y

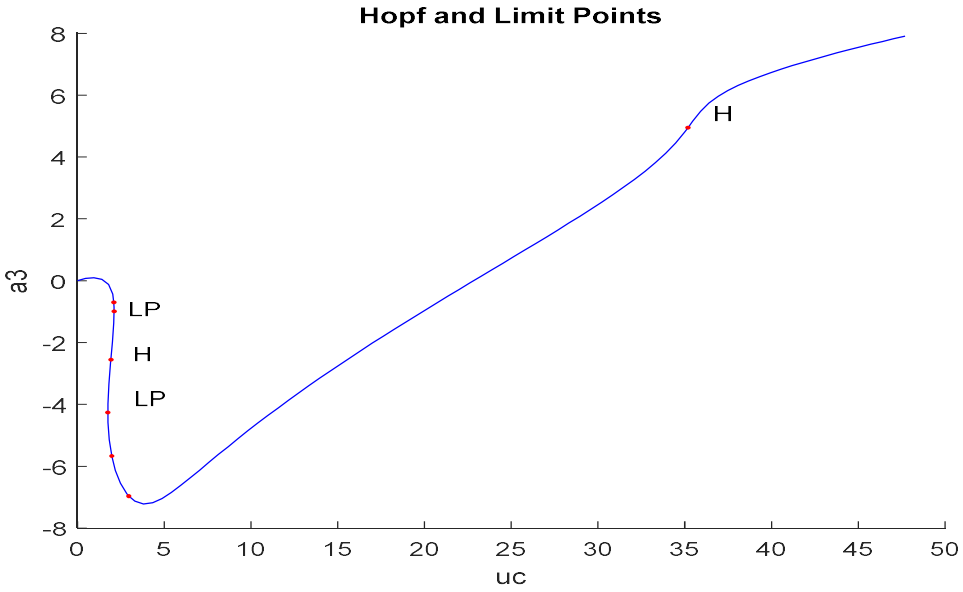

Fig. 1a Hopf Bifurcation and Limit Points

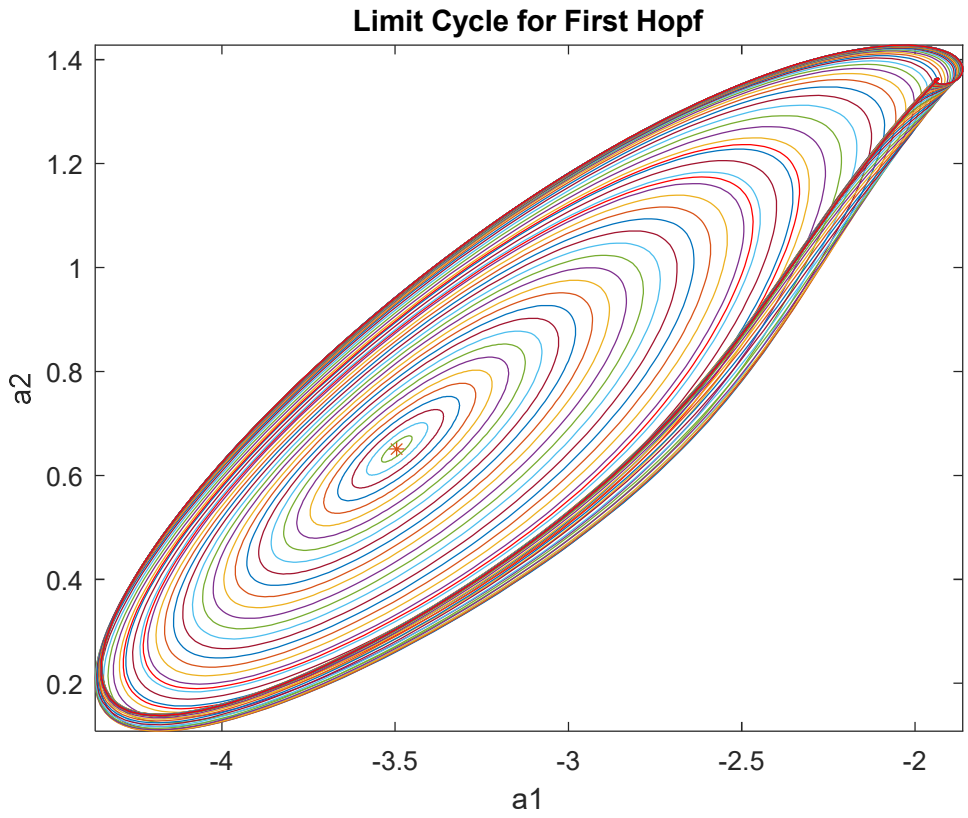

Fig. 1b Limit Cycle for first Hopf Bifurcation

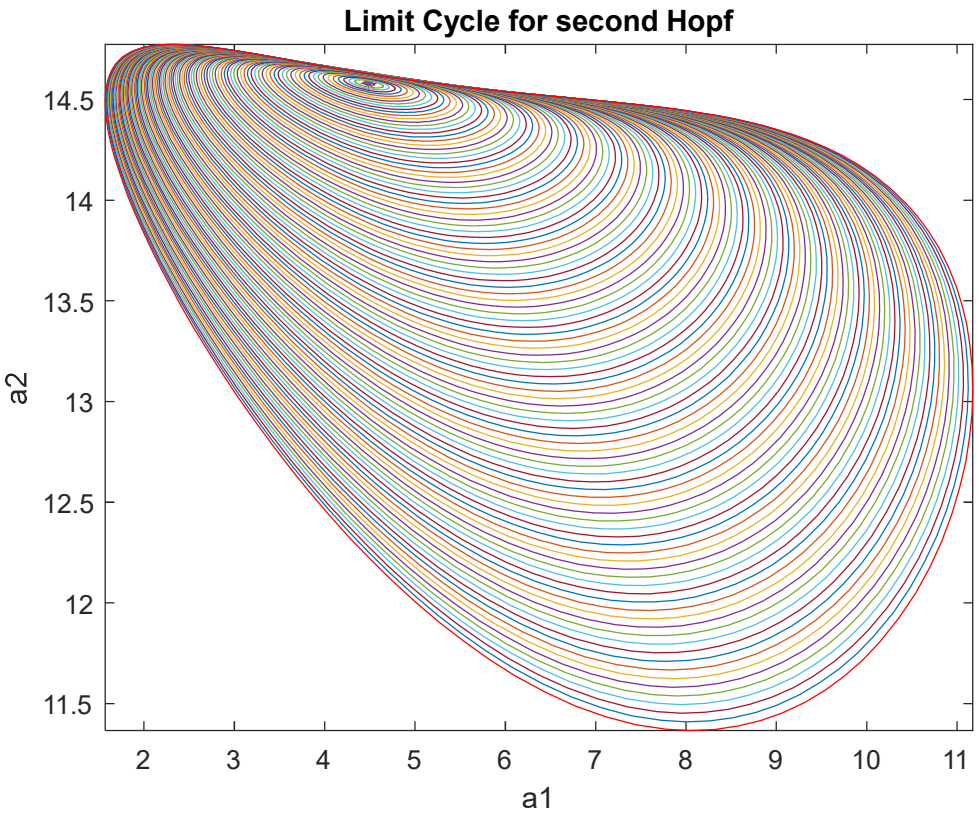

Fig. 1c Limit Cycle for second Hopf Bifurcation

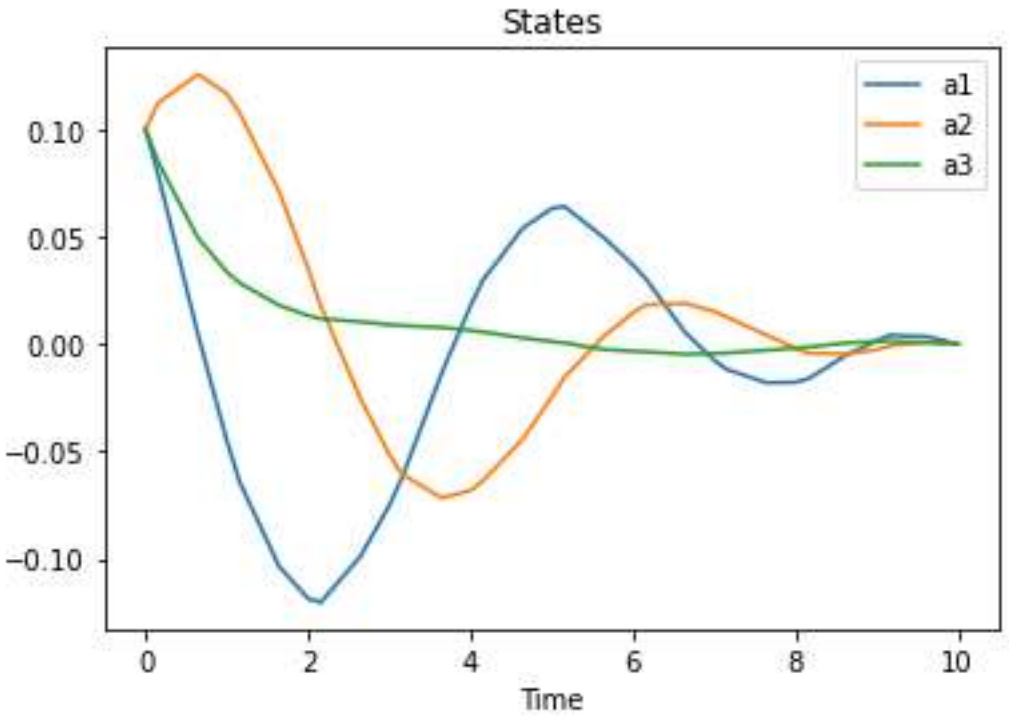

Fig. 2a Optimal control with no Hopf constraint a1, a2, a3

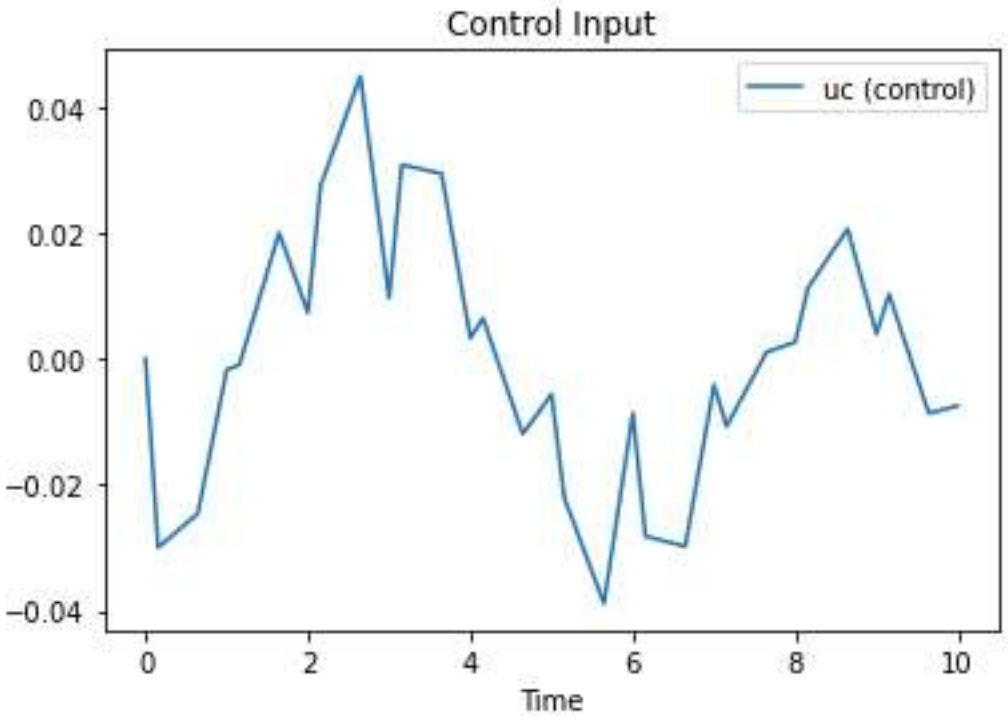

Fig. 2b Optimal control with no Hopf constraint uc

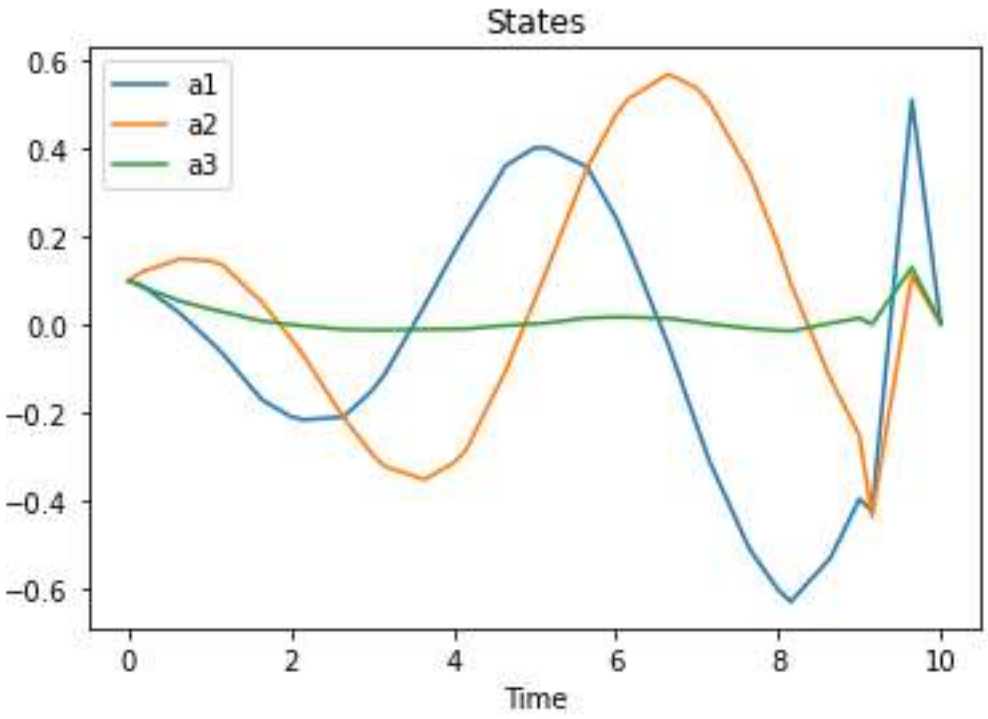

Fig. 2c Optimal control with Hopf constraint a1, a2, a3

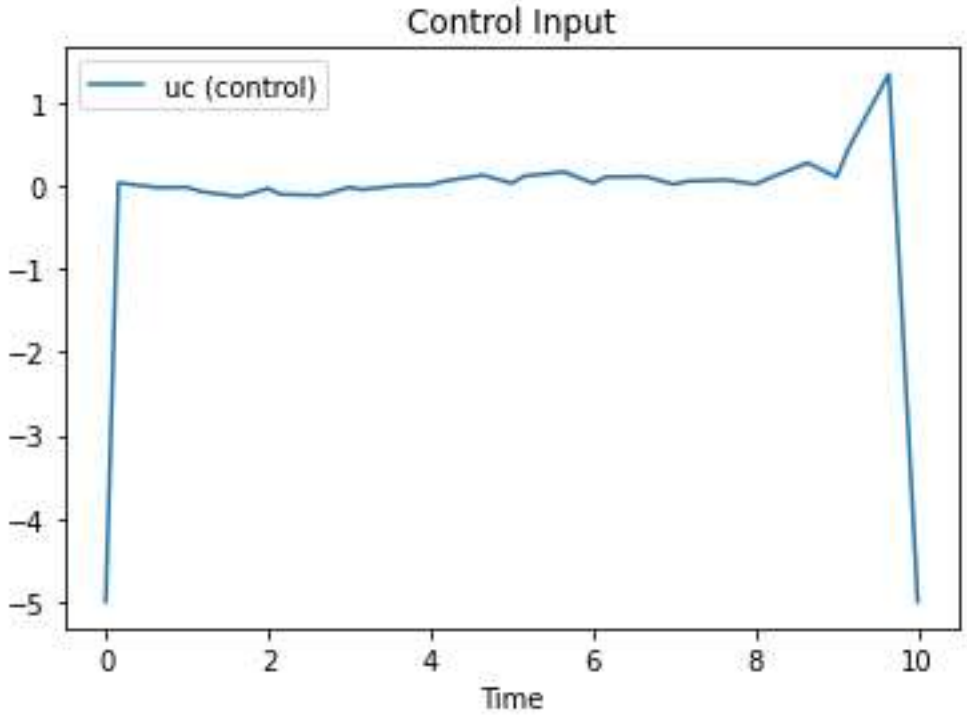

Fig. 2d Optimal control with Hopf constraint uc